The Design & Development of the Ocean Color Instrument

Precision Superduplex Hybrid Bearing Cartridge

Joseph Schepis*, Timothy Woodard**, Claef Hakun*, Konrad Bergandy*, Joseph Church*,

Peter Ward**, Michael Lee**; Alfred Conti***; Jeffrey Guzek****

Abstract

A high precision, high-resolution Ocean Color Imaging (OCI) instrument is under development for the Plankton, Aerosol, Cloud, ocean Ecosystem (PACE) mission which requires a pair of medium speed mechanisms to scan the ocean surface continuously. The design of the rotating telescope (RT) mechanism operating at 360 RPM and the half-angle mirror (HAM) mechanism synchronized at 180 RPM was concern for maintaining pointing precision over the required life and continuous operations. An effort was undertaken with the manufacturer to design and analyze a special bearing configuration to minimize axial and radial runout, minimize torque, and maintain nominal contact stresses and stiffness over the operating temperature range and to maximize life. The bearing design, analysis, development and testing along with the design specific technical challenges imposed upon mechanism engineers will be discussed. Bearing performance, runout as achieved and verified during encoder installation and operating torque will be described.

Introduction

PACE will extend the high quality ocean ecological, ocean biogeochemical, cloud, and aerosol particle data records begun by NASA in the 1990s, building on the heritage of the Sea-Viewing Wide Field-of-View Sensor (SeaWiFS), the Moderate Resolution Imaging Spectroradiometer (MODIS), the Multi-angle Imaging SpectroRadiometer (MISR), and the Visible Infrared Imaging Radiometer Suite (VIIRS). The mission will be capable of collecting radiometric and polarimetric measurements of the ocean and atmosphere, from which biological, biogeochemical, and physical properties will be determined.

The PACE observatory is comprised of two instruments, an Ocean Color Instrument (OCI), Figure 1, and a Multi Angle Polarimeter (MAP). The OCI is the primary instrument on the observatory and is being developed at GSFC. The OCI is a hyper-spectral scanning (HSS) radiometer designed to measure spectral radiances from the ultraviolet to shortwave infrared (SWIR) to enable advanced ocean color and heritage cloud and aerosol particle science. OCI accomplishes its mission objectives by implementing an RT mechanism, rotating at 360 RPM, and phased-locked to the HAM mechanism rotating at half the RT speed. These

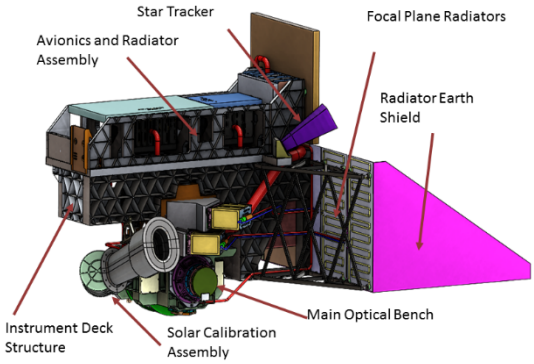

Figure 1 - OCI Configuration

* NASA Goddard Space Flight Center, Greenbelt, Maryland
** The Aerospace Corp, El Segundo, California
*** The Barden Corp, Danbury, Connecticut
**** Design Interface, Columbia, Maryland

Proceedings of the 44th Aerospace Mechanisms Symposium, NASA Glenn Research Center, May 16-18, 2018

synchronized mechanisms scan ocean surfaces with 1000 m resolution and 20 m track-to-track overlap. The PACE satellite is planned to be launched in 2022-2023. [1, 2]

Mechanism Operating Requirements

The RT and HAM are precision mechanisms spinning synchronously to scan the ocean surface and place the optical image through the OCI slit. The requirements considered for these mechanism designs include:

- Speed: 360 & 180 RPM
- Position: 40 arc-sec knowledge and 10 arc-sec maximum error (2^{15} bits), sampling at 50 KHz
- Life: ground testing + 3 months in-orbit commissioning + 3 years continuous on-orbit operations
- Torque: minimize mechanical power to minimize thermal conditions at the bearing and for minimizing control electronics overhead
- Mechanical Loads
    - Structural: worst case launch vehicle mass acceleration curve (MAC), 42g, for mechanisms; sine vibration 10g from 5-100 Hz
    - Thermal: 10C to 30C qualification range, including self-generated heat

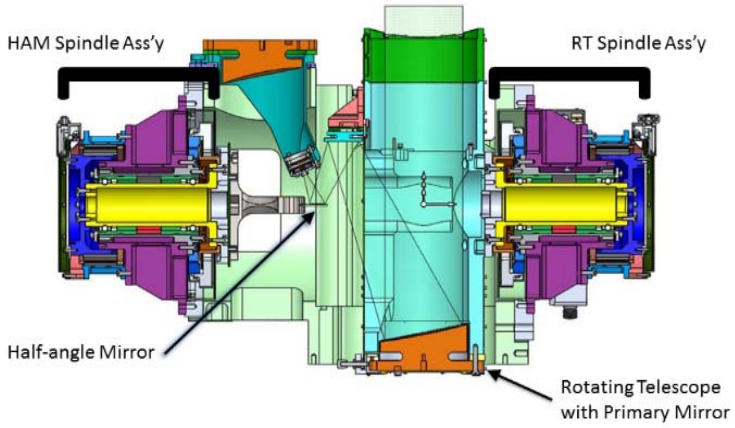

Figure 2 - RT and HAM Mounted on Main Optical Bench

Runout: Challenges to Meet Requirements

Minimizing the axial and radial runouts were primarily driven by the optical system sensitivity estimates and the need to meet challenging pointing requirements. Both synchronous runout and asynchronous runout had to be minimized to keep the bearing cartridge runouts within the requirements. The RT and HAM with precision optical encoders mounted to the shaft flange end, their runout requirements were most challenging while the motor and encoder supported by the aft end have slightly relaxed requirements. The cartridge total indicator runout (TIR) requirements are given in Table 1. As these were very challenging requirements, the bearing vendor was taking all reasonable steps necessary within their capabilities to achieve these values while operating in a "best effort" mode.

Table 1 – TIR Runout Requirements

	Shaft Flange End	Aft End	Outer Races (ea.)
Radial Runout	2.54 µm (100 µ-in)	2.54 µm (100 µ-in)	0.51 µm (20 µ-in)
Axial Runout	1.27 µm (50 µ-in)	5.08 µm (200 µ-in)	NA

These challenging requirements meant that the best geometrical precision in bearing races, ball roundness and their potential lobing was required. Additionally, the number of mating surfaces with their inherent errors

due to tolerance buildup had to be minimized. For these reasons the mechanism designers decided not to use commercial off-the-shelf bearing designs but rather to start with no preconception and design a system that maximized the likelihood of success. The cartridge design demanded complete customization that lead to inner races ground on the same grinder setup. There were no shaft fit or concentricity errors because there was no shaft. The outer rings also required very high tolerances that resulted in a hybrid superduplex configuration.

Cartridge Design: To Flange or Not to Flange?

The preliminary design of the RT and HAM were based on a simplified loads assessment of standard 108H angular contact bearings, preloaded as a duplex back-to-back (DB) pair with a 10.16 cm (4.00") row separation. By working with the bearing manufacturer to minimize radial and axial runout, a new cartridge design configuration was developed. The OCI bearing cartridge concept is similar to x-ray bearing cartridges, wherein the inner raceways are ground directly into a shaft and the preload is provided by fitting a spacer between wide outer rings. The spacer is essentially in a "C" shape to facilitate assembly. This entire preloaded cartridge can be fitted into a housing structure and clamped into position. The bearing manufactuer has experience building this type of bearing cartridge.

The detailed design included selection of contact angle, material, and fits. Material selection was dominated by the launch load demands and other qualitative considerations. Two contact angles were considered: 15° and 25°. The 25° contact angle offered lower contact stress due to preload and better axial capability with a slight decrease in radial capability and no truncation issues. Though a tighter raceway curvature could be used to decrease operating contact stress and increase the load capacity, a looser raceway curvature provides a lower running torque given the smaller contact area.

The initial target preloads evaluated were 111N (25 lbf), 267N (60 lbf), and 445N (100 lbf). The 267N preload offered the best balance between protection during launch and operating contact stress. The as-built bearing cartridge is shown in Figure 3.

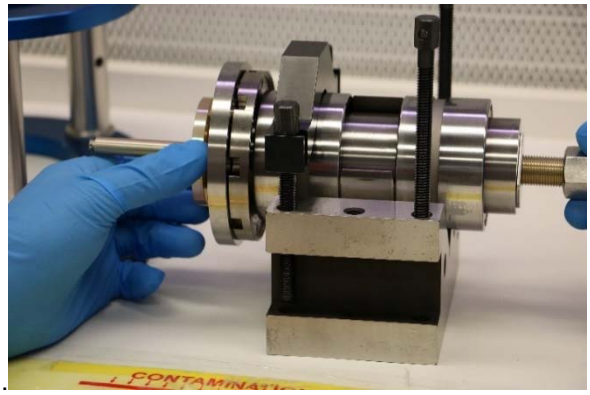

Figure 3 - Bearing Cartridge Showing Captured Titanium Mounting Collar (Floating)

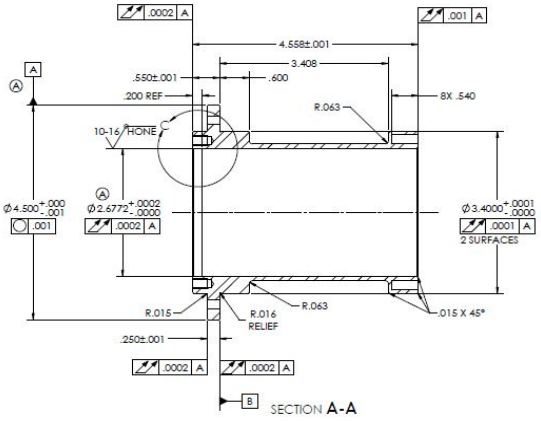

Figure 4 - Flanged Sleeve

While material selection will be discussed next, that selection process did indeed have a direct effect on the design. Disregarding material concerns for the moment, the original design concept was to implement a mounting flange on the forward (shaft flanged end) outer ring. The original material consideration of M62 brought with it a concern and a reality of limited supply stock size options. Due to that reason, combined with requiring different designs for the two outer rings (and the increased cost of such) drove the design away from a flanged cartridge. This required the use of the sleeve to mount the cartridge into the mechanism housing. When the material choice later led to 440C, this decision was not revisited. The result of the flange question was for the mechanism team to implement "sleeving". The sleeve provides a method for mounting

the cartridge into the aluminum mechanism housing, which also provide structural support for the encoder read heads and motor stator. In order for the sleeve to provide maximum performance enhancement for the RT and HAM assemblies it must: 1) be a relatively close coefficient of thermal expansion (CTE) match; 2) be relatively easy to thermally control; 3) have precision interfaces (fits) to the cartridge and the housing and 4) must completely capture the cartridge.

The cartridge basic outer diameter and sleeve bore are 67.75 mm (2.6772”). The sleeve bore runout is specified as 5.08μm (0.0002”). Cartridge to sleeve fit up design values are given in Table 2. Fit ups for the sleeve to housing were similar.

Table 2 - Cartridge to Sleeve Fit Up

	Diametric Tolerance		Total Clearance
Cartridge	+0.00 μm	(+0.0000”)	Line-to-line, min 7.62 μm (0.0003”), max
	-2.54 μm	(-0.00001”)	
Sleeve	+5.08 μm	(+0.0002”)	
	-0.00 μm	(-0.0000”)	

Thermal control of the cartridge is accomplished by mounting a flexible, wrap-around Kapton® heating element on the exterior mid-section of the sleeve. Test thermocouples and flight thermistors were also installed for heater control and telemetry. The sleeve is shown in cross-section in Figure 4. Capturing the cartridge in the sleeve was completed with a customer supplied titanium mounting collar that was “captured” between the rotating shafts and fixed outer forward outer races during clean assembly. At the aft end of the sleeve, a tabbed collar was mounted such that there was axial compression providing a nominal 3.89 KN (875 lbf) clamping force. Sleeve material selection for CTE and machinability will be described in the next section.

Material Choices

Materials considered for the bearing rings included M62 tool steel (Rex/CRU20 crucible steel) and 440C stainless steel. The M62 tool steel has a higher allowable contact stress than 440C (Table 3), which potentially allows the use of a smaller bearing. A smaller bearing would lower the running torque, weight, and stiffness. For the same geometry and load, the M62 bearing would operate at a higher contact stress with a correspondingly smaller contact area. The 440C stainless steel is more available and is a common bearing steel, which lowers risks associated with supply and specialized processing. Ultimately, the 440C was able to provide adequate load capacity with the initially determined bearing size and M62 was not used. This choice assured material availability and reduced risks associated with specialized material processing at the cost of reduced stiffness and lower load capacity.

The ball materials considered were 440C stainless steel or silicon nitride ceramic (Si_3N_4). The silicon nitride ball offers several benefits of enhanced lubricant life, lighter weight, and higher stiffness at the expense of significantly different coefficient of thermal expansion compared to the steel rings [3, 4, 5, 6]. The additional change in preload over temperature due to a difference in material thermal expansion coefficients was determined by analysis to be an acceptable detriment, given the other benefits of silicon nitride.

The sleeve material of 440C stainless steel was used in order to minimize thermal expansion coefficient differences between bearing rings and the sleeve (Table 4). The sleeved cartridge fits into an aluminum housing, which provides the structural connection to the instrument optical bench. With precision fits, the separation and support provided by the stainless steel sleeve minimizes the effect of the thermal expansion coefficient differences between the steel bearing and aluminum housing.

Table 3 - Bearing Component Material Properties

	M62	440C	Si3N4
Allowable Max Contact Stress	3790 MPa (550 ksi)	2310 MPa (335 ksi)	n/a
Modulus	235 GPa (34.1e6 psi)	205 GPa (29.7e6 psi)	320 GPa (46.4e6 psi)
Poisson's Ratio	0.29	0.283	0.26
Density / Specific Gravity	8.17 g/cc (0.295 lbm/in^3)	7.8 g/cc (0.282 lbm/in^3)	3.16 g/cc (0.114 lbm/in^3)
Thermal Expansion Coefficient	10.66e-6 1/C	10.2e-6 1/C	2.9e-6 1/C
Type	Tool Steel	Stainless Steel	Ceramic
Expected Hardness	RC 65	RC 61	HV 1550

Table 4 - Structural Component Material Properties

	Al 6061-T6	440C	Ti-6Al-4V
Modulus	69 GPa	205 GPa	114 GPa
Poisson's Ratio	0.33	0.283	0.33
Density/Specific Gravity	2.7 g/cc (0.098 lbm/in^3)	7.8 g/cc (0.282 lbm/in^3)	4.43 g/cc (0.16 lbm/in^3)
Thermal Expansion Coefficient	23.6e-6 1/C	10.2e-6 1/C	8.6e-6 1/C
Type	Aluminum	Stainless Steel	Titanium

The ball retainer material is machined phenolic, MIL-I-24768, Type FBE, often used in many space applications due to its light weight and ability to be properly impregnated with the lubricating oil, acting as an oil reserve. To provide additional lubrication reservoirs, Nysorb® rings, also impregnated with oil were designed to fit into outer race inner grooves.

Analysis Approach

A bearing analysis was conducted to ensure that the assembled and integrated bearing cartridge would meet design and performance requirements. This analysis was performed concurrently with detailed design of the cartridge to aid final design decisions, such as material selection and fits. The analysis ensured that two primary requirements were met: the maximum mean contact stress in the bearing must be within allowable limits during launch and the final preload range during operation was suitable for the rotating telescope. The goal was to have an appropriate preload range over the expected operating temperatures, and given the manufacturing tolerances of the piece parts. A higher preload means a shorter fatigue life and higher drag torque, while a lower preload might compromise the stiffness of the system. An example preload goal range might be between 44.5N (10 lbf) and 445N (100 lbf) preload. The analysis also ensured no truncation of the contact ellipse on the land, as well as provided estimates for running torque and stiffness.

Key parameters which affect the analysis results include:

- Material properties (Young’s modulus, Poisson’s ratio, coefficient of thermal expansion)
- Bearing geometry (bearing size, raceway curvature, contact angle, straddle)

- Mounting (clamping force, interference fits, initial preload)
- Operating parameters (temperatures, speed, launch loads, preload)

With the materials, geometry, and operating parameters fixed, the final design decisions were related to the mounting of the bearing into the sleeve and housing. Therefore, this bearing concept described above leads to a number of issues that must be accounted for in the detailed design and mounting analysis:

- Clamping effect on preload
- C-spacer effect on raceway parallelism
- Sleeve fitting effect on preload
- Sleeve/housing fit

Clamping effect on preload:

The bearing integration concept calls for the bearing cartridge, which consists of the outer rings preloaded with the C-spacer and shaft, to be clamped into the bearing sleeve. The clamping rings squeeze the outer rings together, compressing the outer rings and the C-spacer. Since the outer rings are being compressed, the outer raceways move closer together which lowers the preload. The compression also increases the diameter of the raceways due to Poisson's effect. This axial displacement of the raceway and increase in diameter of the rings are included in the bearing mechanical analysis via a change in the initial preload and change in fit.

C-Spacer effect on raceway parallelism:

The circumferential gap in the C-spacer caused an uneven distribution of the preload on the inner face of the outer rings. Although the clamping ring was contacting the entire face of the outer ring, the C-spacer only supported a section of the outer ring; this caused a variation in axial displacement of the outer raceway. The concern was a loss of parallelism between the outer raceways. Finite Element Analysis (FEA) was used to evaluate raceway parallelism affected by the C-spacer as shown in Figure 5. The worst case difference in axial displacement due to clamping of any point on the raceway was predicted by the FEA to be around 525 µm (0.000021 in).

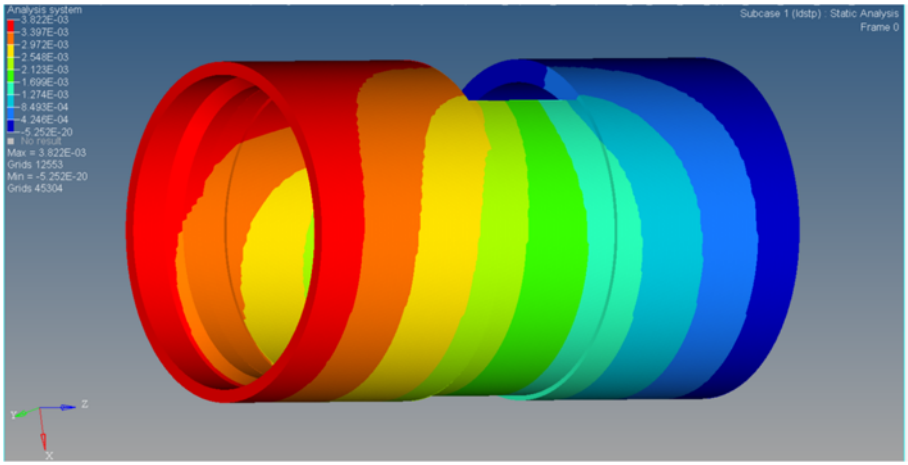

Figure 5 - FEM Results Showing Deformation of the Outer Rings Due to Clamping Load

Sleeve fitting effect on preload:

As it is well known in the bearing field, an interference fit of the outer rings in the sleeve increases preload by compressing the rings and decreasing the radial play. This decrease in radial play is seen by the preloaded bearing as a change in preload and contact angle.

Mechanism housing fit effect on sleeve fit:

The interference fit of the sleeve into the mechanism housing affects the sleeve diameter in turn also affects the bearing/sleeve fit.

Analysis process:

The BRGS10C software was used for the bearing internal mechanical analysis and Python for scripting and cartridge mounting mechanical analysis. The process had to take into account the effects mentioned above. The bearing mechanical analysis software BRGS10C was originally created for analyzing directly adjacent preloaded pairs with conventional housings, shafts, and clamping. BRSG10C cannot on its own properly analyze the complex mounting of a cartridge such as the OCI concept. The Python scripting was able to account for the unique mounting concept as well as provide a means of iterating through the entire design space quickly. The ability to iterate through all design configurations allowed a better understanding of each parameter's effect on the final configuration. The adopted analysis process include the following steps:

1. Apply a temperature
    - *Survival cold, cold, room temp, hot, survival hot*
    - *Calculate new part geometries*
2. Apply a sleeve clamping load (based on allowable C-spacer deformation)
    - *3.34, 3.89 & 4.45KN (750, 875, & 1000 lbf)*
    - *Find axial displacement of raceway due to compression (at temperature)*
    - *Find Poisson's effect on outer diameter (at temperature)*
3. Apply housing-sleeve fit
    - *0.0000 to 5.08µm (0.0002 in) interference*
    - *Calculate change in fit between sleeve & bearing*
4. Apply sleeve-bearing interference fit
    - *-7.62µm (-0.0003 in) to 0.0000 clearance*
    - *Adjust fit due to Poisson's effect from clamping & housing fit*
5. Adjust preload due to clamping compression (based on axial stiffness)
6. Run BRGS10C with adjusted preload & sleeve-bearing fit
7. Report results:
    - *Final preload*
    - *Maximum mean stress*
    - *Stiffness / Displacement*
    - *Truncation*

This process was followed for each combination of design parameters to determine their effect on final preload, contact stress, and stiffness. The information was plotted in order to examine the entire design space, as well as to determine each parameter's effect on the result. In this way, the best decision could be made regarding the final fit, clamping load, and initial preload.

Analysis results:

The analysis process provided results for each combination of detailed parameters. Figure 6 shows maximum mean contact stress results for the worst case fits and clamping configuration given a combination of axial and radial loads.

Figure *7* shows the final preload variation for all temperature, sleeve fit, housing fit, and clamping combinations considered. At colder temperatures, the shrinking sleeve and housing fits, along with the silicon nitride ball, cause a rise in preload. Figure 8 shows the maximum mean contact stress for launch and operational cases. Though a lower operating contact stress in desirable, the changes seen given the mounting parameters considered are no cause for significant alarm.

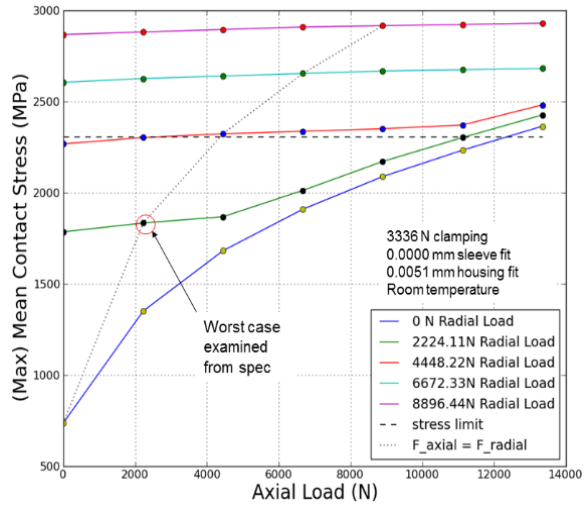

Figure 6 - Contact Stress Capability vs. Radial and Axial Load Cases

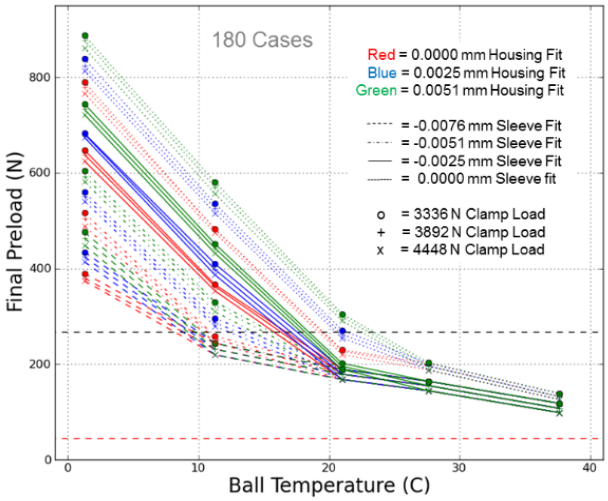

Figure 7 - Final Mounted Preload Variation

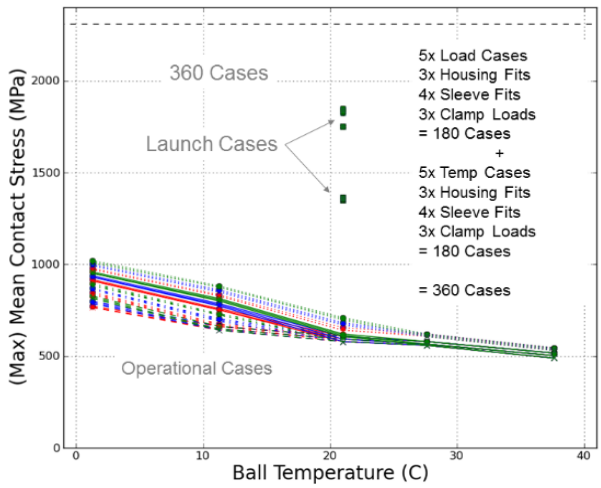

Figure 8 - Maximum Mean Stress for Launch and Operational Case

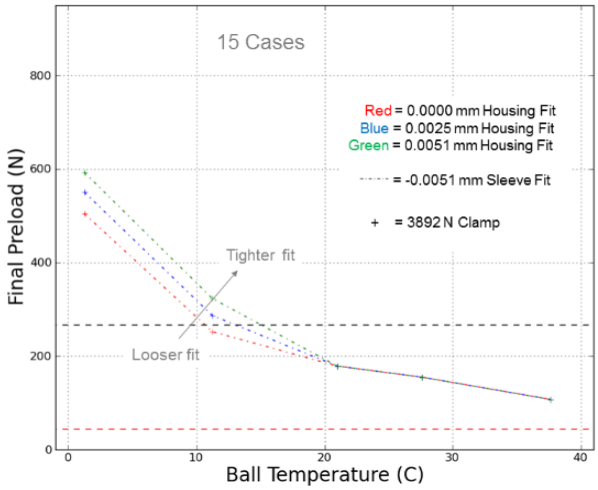

Figure 9 - Effect of Housing Fit on Final Preload

In order to allow a better understanding of each parameter's effect on the results, series of cases were run where certain parameters were held constant, and only one varied. The effect of the varied parameter can then be directly determined by examining the obtained result. Figure 9 shows the effect of housing fit on final mounted preload, given a loose sleeve fit and 3.89KN (875 lbf) clamping force. Only at colder temperatures does the housing fit affect preload.

Figure 10 shows the change in preload due to varying sleeve fit over temperature, given a nominal housing fit. As the figure shows, the sleeve fit has a greater influence on the final preload than the housing fit. This made sense because the sleeve is closer to the raceways and is made of a stiffer material.

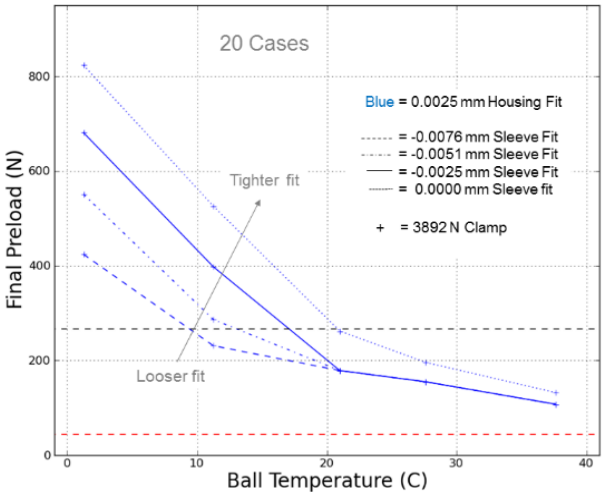

Figure 10 - Change in Final Preload Due to Sleeve Fit, Given a Loose Housing Fit

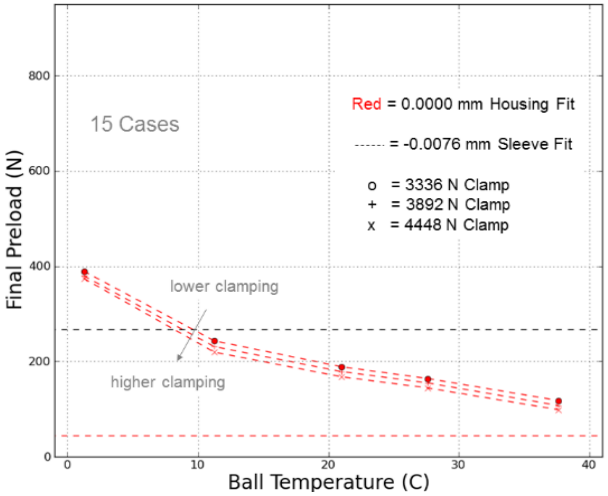

Figure 11 - Change in Final Preload Due to Outer Ring Clamping

Figure 11 shows the effect of clamping on the final preload. The effect is fairly consistent over the temperature range and is a smaller effect than the sleeve of housing fits.

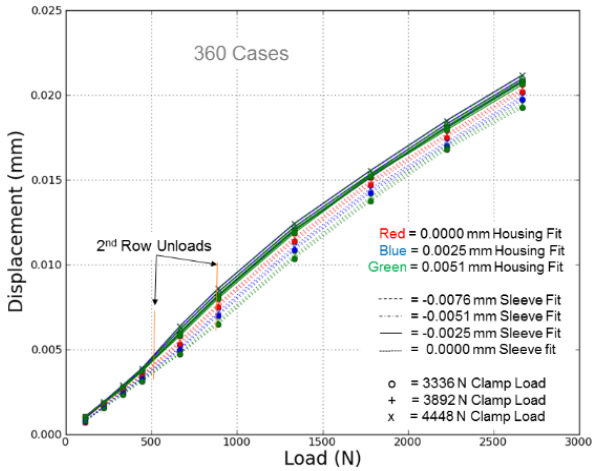

Figure 12 – Axial Load Displacement

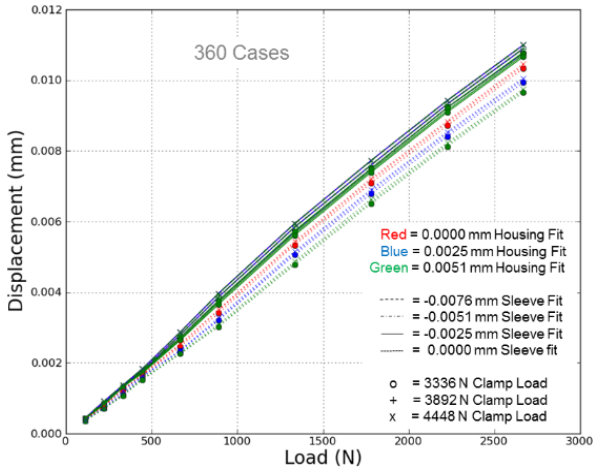

Figure 13 – Radial Load Displacement

Figure 12 and Figure 13 show the load-displacement relationship for axial and radial loads, respectively. The change in the shape of the curve clearly shows where the front row unloads for the axial load case.

Given the numerous design parameters and the likelihood of achieving such close tolerances on each of those parameters, the ability to create permutations through each range, and evaluate the effect of each tolerance, gave increased confidence in the performance of the fully assembled bearing.

Lubrication

The bearing cartridge is assembled after being lightly lubricated with Nye Lubricants 2001 synthetic oil. Nye 2001 has proven itself to be a reliable space lubricant as long as enough lubricant is available to the bearing. NyeBar®-P oil barrier films are added to each end of the cartridge to reduce oil migration from the bearing. A Nyesorb™ lubricant reservoir in each outer ring ensures lubricant is available through lifetime of the mechanism. Cages and reservoirs are vacuum impregnated with lubricant and weighed prior to assembly to ensure oil take-up. A life test will be conducted to ensure adequate lubricant life for the OCI design and operating conditions.

It should be noted that the use of the silicon nitride balls and its material dissimilarity to its friction couple, steel, has shown remarkable lubrication life extensions in other applications and has for years, allowed the luxury of using just oil in critical applications that require extreme torque quietness over extended periods of time. The oil is not damaged as fast as with all steel bearings and therefore extra grease or grease dams for life extension are not needed. The lubricant life tests, discussed in a later section, should bear this conclusion out and provide more real data for the aerospace mechanism community.

Cartridge Runout Verification

To measure and document the axial and radial runout requirements given in Table 1, the bearing vendor developed new test hardware to verify cartridge performance. A non-contacting, capacitive picometer sensor was mounted in adaptable setups to determine synchronous and asynchronous TIR at the four specified interfaces and at both 360 and 180 RPM. Initial setups indicated that external electrical and mechanical noise, structural modes and sensor surface squareness, generally in that order of effect, were all contributors to significant measurement error. By diligent effort, all error sources were eliminated.

Electrical noise was addressed by establishing a thorough grounding scheme, as well as by establishing an electrically “quiet” facility location and controlling local equipment usage. Structural noise was addressed by redesigning to a very stiff sensor mounting block and a stiff structural loop between the sensor and cartridge mounts. The motor drive signature was isolated using a pulley with an O-ring driving a jack shaft supported by Rulon bearings then coupled to the cartridge with Tygon tubing. By attention to sensor positioning, it was noted that the surface squareness of the sensor relative to the cartridge could be altered by indexing (i.e., rotating on axis) the transducer body by 90° to 270°. The sensor output was sent to a dual trace spectrum analyzer to display the displacement in time and frequency components. After corrective actions, by taking a time trace reading with no shaft motion, static sensor readings in all four locations indicated approximately 0.0127 μm (0.5 μ-inch) noise. During high speed shaft rotations, sensor displacement vs. time gave us a total runout (synchronous and asynchronous) and the frequency trace served to distinguish between synchronous and asynchronous runout. The result was that virtually all runout was synchronous (that is, on the orders of rotations).

Cartridge Performance Predictions and Verifications

Performance predictions

During the superduplex cartridge fabrication, an effort was begun to predict starting and running torque at 360 RPM for inclusion in the drive electronics design capability. To that end, analysis and tests were used to predict performance. Generally, bearing torque consists of a load torque caused by sliding and rolling friction between components in the bearing, and a viscous torque, due to the plowing and squeezing of the lubricant. The load torque is largely dependent on loading, and weakly dependent on speed, while the viscous torque is largely dependent on speed, and weakly dependent on load. Both BRSG10 and ORBIS bearing analysis codes provide similar estimations of load torque at zero speed, as show in Table 5, given the same assumption of coefficient of friction.

Table 5 - Load and Speed Torque Predictions

	BRGS10	ORBIS	units
Load Torque Est. mu = 0.08, P = 60 [lb]	6.9 (0.974)	6.8 (0.96)	mN-m (in-oz)
Viscous Torque Est. 350 cSt, LQF = 0.3	39.5 (5.6)	25.4 (3.6)	mN-m (in-oz)
Viscous Torque Est. 240 cSt, LQF = 0.3	30.1 (4.35)	19.9 (2.82)	mN-m (in-oz)

The viscous torque is affected by the lubricant viscosity and quantity of lubricant in the bearing. The lubricant viscosity is affected by temperature while the quantity of lubricant and its effect on torque is dependent on the size of the bearing, type of lubricant, and other miscellaneous factors. This leads to an empirical factor, called lubricant quantity factor (LQF) used in viscous torque estimation and the need for testing to anchor the analysis. The viscous torque estimates can be found in Table 5, for BRSG10 and ORBIS. The ORBIS values are lower because of its use of dynamic rather than kinematic viscosity, and because of BRGS10's addition of a ball factor, which is the number of balls divided by 10. When corrected for these differences, the estimation differs by less than 2 percent.

In addition, a pair of off-the-shelf 108H bearings were disassembled and cleaned, then reassembled with Nye 2001A oil impregnated phenolic retainers and ceramic balls. These bearings were then preloaded in a back-to-back configuration and verified with an in-situ load cell. Here, the lubricant condition was duplicated to what was to be the actual cartridge condition. The oil meniscus between ball and race in this test was visually identical to final assembled cartridges. Once assembled into a torque test rig, starting and running torque were measured as a function of preload.

The 108H bearings were subjected to Coulomb (starting) torque measurements at various preloading values, as shown in Figure 14, with the slope and y-intercept identified. Notice that if the negligible y-intercept value is ignored, the starting torque is the slope of the curve multiplied by the preload force. As such, the slope is an alternative form for the friction coefficient, in this case, μ = 0.0152.

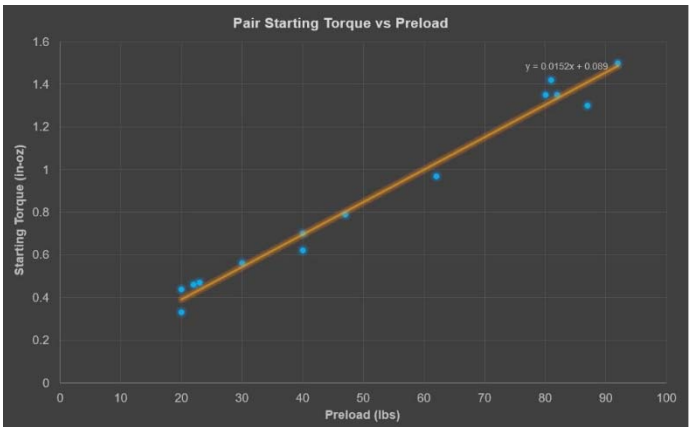

Figure 14 - 108 Pair Starting Torque vs Preload (Note: units are in lb and oz•in)

Running torque as a function of time can be seen in Figure 15. This data shows that the viscous torque is clearly associated with speed, as shown in the data where the speed was changed and the torque changed respectively. Here the effect of run in can be dramatically seen, over 47 minutes of running the torque reduced from 56 mN•m (8 oz•in) to 39 mN•m (5.5 oz•in). This data also shows that the viscous torque is only weakly associated with preload, as shown with the changes in preload but only minor changes in torque give the same speed.

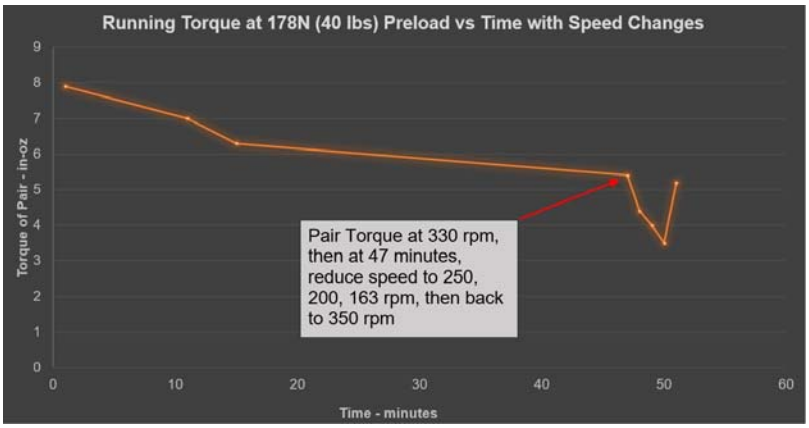

Figure 15 - Torque vs. Time Test Results (Note: units are oz•in)

As-Built Cartridge Torque Performance

Prior to shipping from the manufacturer, the bearings were torque tested on a Vibrac machine. Torque data is typically captured during 0.5 RPM to 2 RPM rotations. Example results can be seen in Figure 16 and summarized in Table 6. This data shows that the low speed torque for the cartridge is about 50 percent higher than expected from analysis or off-the-shelf testing. This means that 1) the preload is higher than expected, 2) the coefficient of friction is higher than expected, or 3) the viscous contribution at low speed is higher than expected. Torque testing, then, is necessary to ground / anchor torque estimation, given the many empirical factors included in torque estimation methods.

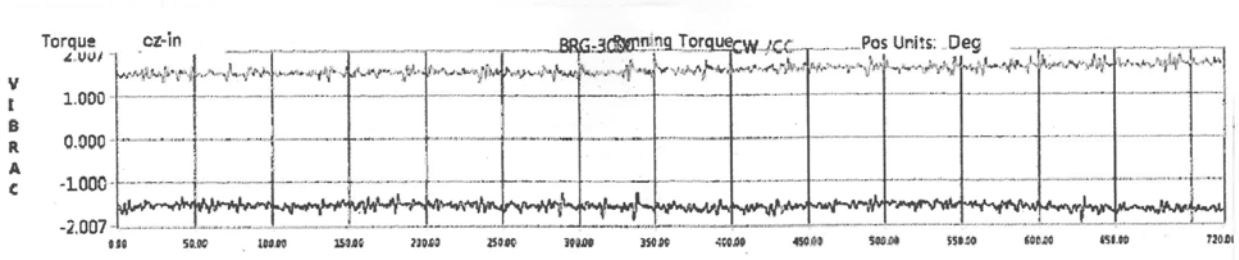

Figure 16 - VIBRAC Running Torque Test on SN 006, Typical (Note: units are oz•in)

Table 6 - SN 006 Torque Test Summary

	CW	CCW	Units
Peak Torque	-14.17 (-2.007)	13.76 (1.949)	mN•m (oz•in)
Average Running Torque	-11.21 (-1.588)	11.21 (1.588)	mN•m (oz•in)
Maximum Hash Width	4.44 (0.629)	2.75 (0.389)	mN•m (oz•in)
Average Hash Width	2.27 (0.322)	0.71 (0.101)	mN•m (oz•in)

Spindle Assembly and Thermal Conditioning

Spindle assembly appeared simpler “on paper” but was more difficult in the practice due to the tight tolerances. Pre-assembly steps included precision cleaning of the sleeve, housing and flexible clamp as well as installation of the thermal control hardware onto the sleeve. The sleeve bore was carefully inspected for internal surface abnormalities. The sleeve bore was lubricated with a light film of Nye 2001 oil with a clean swab and then the heater leads were connected to a 30V power supply to expand the sleeve for

installation. Since the assembly was taking place in the swift moving, cool air of a flow bench (ISO 14644-1 Class 5), the sleeve in its support stand was covered to reduce convection losses. During the heating process, the exterior of the bearing cartridge was also coated with a thin film of Nye oil and placed in a flange up orientation to allow any excess oil to pool on the lead in edges of the cartridge. Once the sleeve temperature, as measured by a thermistor at the flange end, reached 50-55°C the cartridge was manually suspended over the sleeve at the lead in and dropped in. Being that the cartridge and sleeve are the same material (and CTE) and have a very tight tolerance, binding was always a concern. While the first of five assemblies resulted in a cartridge seizing with only a small fraction of the cartridge passed the lead in, the remaining four cartridges dropped in flawlessly, guided be the expert hands of our assembly technicians. The partially installed cartridge was bagged along with the sleeve and support stand and pressed into position on a tension testing machine with approximately 534N (120 lbf) load. The collar fasteners were installed and torqued to fully seat the cartridge. After that, the flex clamp was installed and torqued. Figure 17 shows the thermal control hardware mounted to the sleeve prior to assembly and the cartridge installed and fully seated in the sleeve.

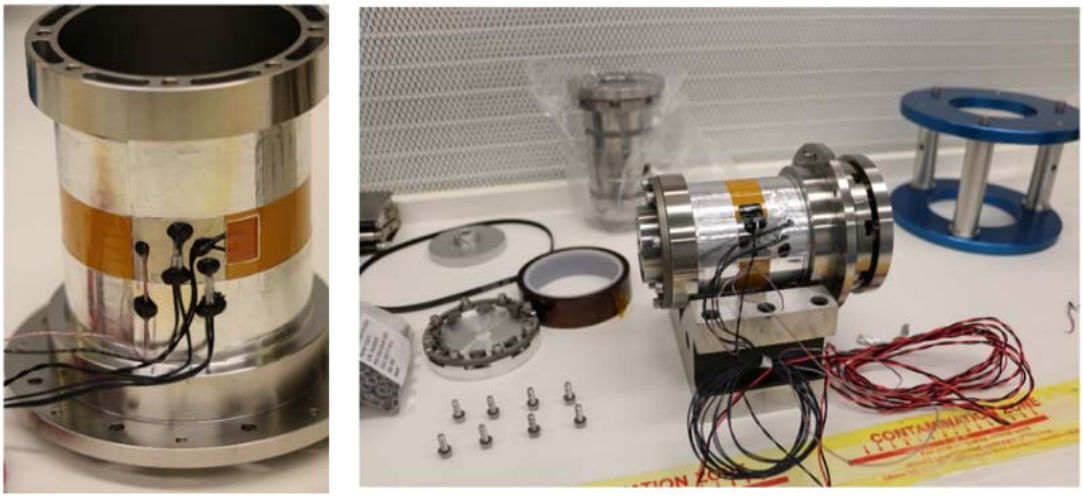

Figure 17 - Flanged sleeve with and without bearing cartridge

Upon completion of the sleeve installation, the housing bore was inspected and lightly lubricated with Nye oil. It was then placed on a ceramic electric heating element until a thermistor registered 65-70°C. During heating, the sleeve external lands were similarly lubricated with Nye oil. The sleeve was dropped into the aluminum housing and registered with its alignment pin without any difficulty. The completed housing assembly is shown being installed in its support stand in Figure 18.

In order to hold repeatable relative position of the encoder code disk and read head, the completed spindles were exposed to thermal conditioning prior to shipment for installing the encoder components.

The spindles were exposed to 12 ½ thermal cycles at ambient pressure over the survival temperature range of 0°C to 40°C. The cycles assure that there is no residual assembly shear stress present due to differential offsets from the shrink fits.

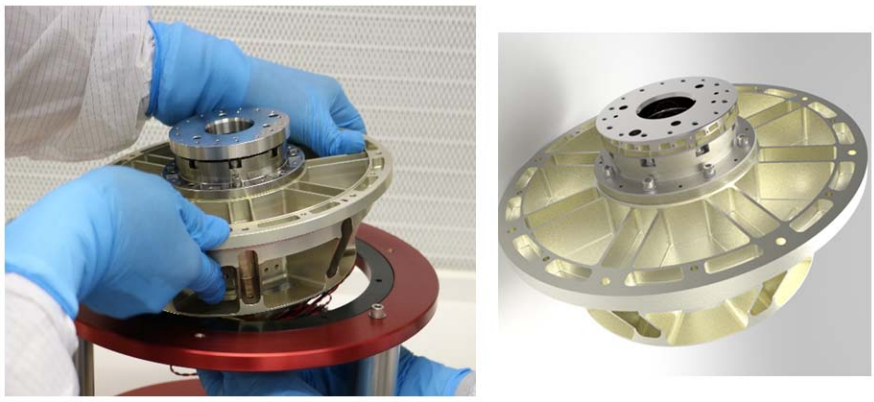

Figure 18 - Assembled spindle (hardware and CAD model)

Spindle Performance

Upon thermal settling cycles, spindle performance testing was undertaken to assure that the assembly mounting had not adversely affected the preload, starting torque, running torque or runout. Drive electronics to be used for spindle testing and the basis for life testing electronics were developed. The mechanism drive electronics (MDE) is capable of commutating a zero cogging torque motor mounted to the flanged end of the spindle based on a 23,600 line optical encoder also mounted on the flanged end. The MDE can accelerate to 360 RPM with the same preliminary profile as is expected for flight. It then runs for a fixed time in order to capture any torque decrease/change as a function of running in and then similarly decelerate. The MDE can operate in low speed dynomometer mode to measure Coulomb friction at 0.5 to 2 RPM.

Figure 19 shows typical low speed torque data for a 5 minute test. The red and blue traces represent motor current captured at 10 Hz and 500 point median filtered data via a MATLAB script. Figure 20 shows the entire torque test results using red and blue traces as described. The data shows a decrease in running torque at 360 RPM from 47.67 mN•m (6.75 oz•in) to 26.83 mN•m (3.8 oz•in) after 1 hour of ambient laboratory operation.

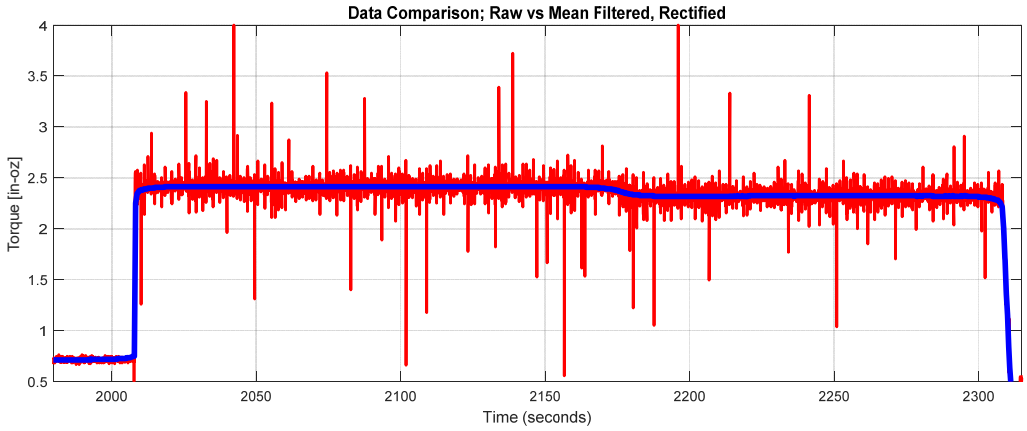

Figure 19 – Spindle Coulomb friction measurement (16.7 mN•m [2.36 oz•in], average; units are oz•in)

Two spindle assemblies were delivered to BEI Precision for high resolution encoder installation. Their installation process usually requires the grinding of the flange mounting interface to the encoder disk to minimize runout and achieve the required accuracy. In this case, BEI responded with confirmation of 0.38-

0.51•10^{-6} m (15-20•10^{-6} inch) runout, axial, including flange surface finish. When coupled to their accuracy tester, 0.33-0.53•10^{-6} m (13-21•10^{-6} inch) runout, axial, and 0.84•10^{-6} m (33•10^{-6} inch), radial, and do not include surface finish. The cartridge performance was “without question, the best bearing assemblies we’ve ever seen” and therefore required no pre-installation grinding.

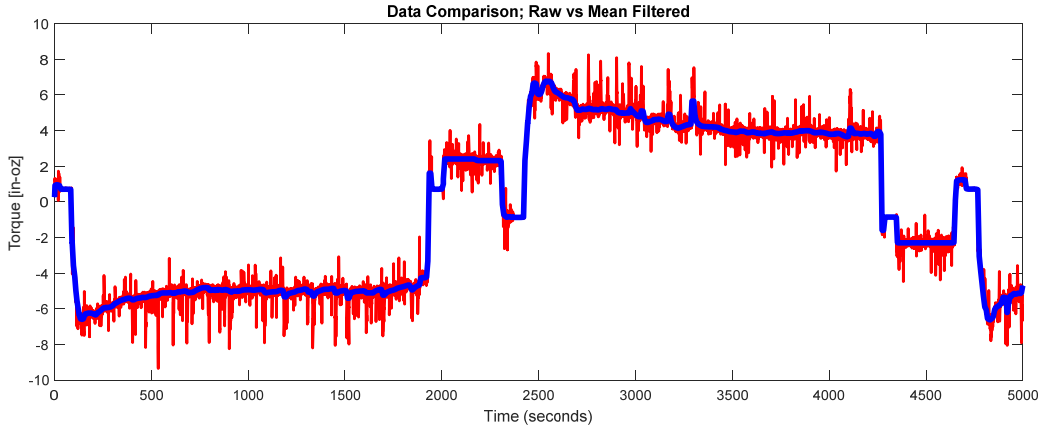

Figure 20 – Spindle torque measurement, ±360 RPM running, ±2 RPM Coulomb (units are oz•in)

Life Testing Plan

A plan has been created to document details of the life testing. The testing will be in two parts to address separate life related risks. The first tests will be of bearings only, abbreviated BOLT (for bearings only life test) and will address the risk of lubricant life and potential degradation. For this test, 6 bearing cartridges have been selected as representative of the lot. They will be installed into 440C sleeves with an appropriate fit, representing flight unit fits, and then installed into stove pipe fixturing representing the mechanism housing, again, with an appropriate fit. Heaters and thermistors will be applied as in the flight configuration allowing us to control the bearings’ bulk temperatures within OCI’s operational range. A life test with multiple units under test (UUTs) allows us to gain the same confidence with fewer cycles than with only one UUT. The UUTs will be fitted with a mass simulator prior to random vibration and sine sweep testing. The mass simulators will be removed and the UUTs will then be installed in pairs into three thermal vacuum (TVAC) chambers sharing a vacuum pump and chiller. The vast majority of testing will consist of operation at 360 RPM as torque is “self-sensed” using the current to a cogless brushless motor. Occasional spin downs to 180 RPM and 2 RPM for Coulomb friction measurements will be performed over the course of the non-accelerated testing. Spin down time testing may also be used to estimate any changes in friction over time.

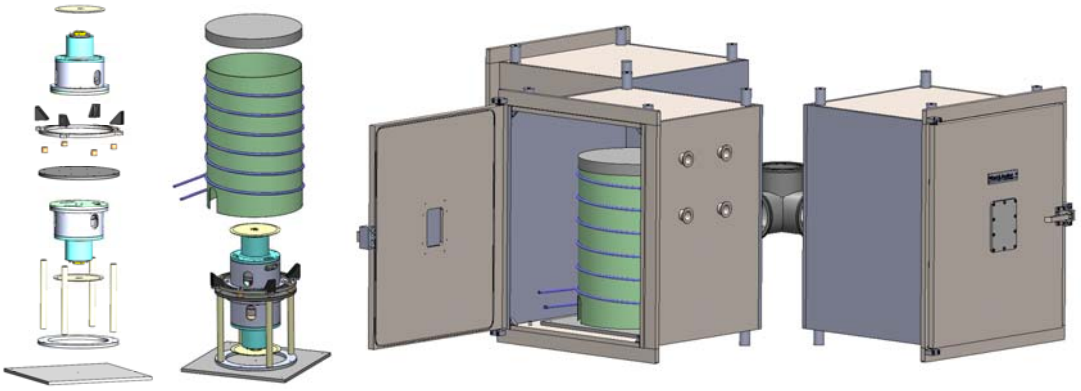

Figure 21 - BOLT Test Configuration

The second test will be of the RT and HAM mechanisms working in synchronization and will address the risk that changes over time will affect the ability of the control electronics to synchronize the relative RT and HAM position and velocity such that the image passes through the instrument optical slit and illuminates the detectors with the required accuracy. These two mechanisms will be configured with an engineering test unit telescope and half-angle mirror and installed on a surrogate optical bench. The UUTs will be subjected to random vibration and sine sweep testing prior to testing in TVAC. This non-accelerated testing is expected to begin in late summer of 2018.

Preparations are underway to assemble the BOLT at the time of writing this paper.

Summary

Some obvious and some not so obvious conclusions can be taken away from the OCI-specific bearing cartridge application design effort. Several key points are summarized as follows:

- Interference fits and their change over temperature have a larger impact on resulting (as installed) preload than outer ring clamping force.
- Ball material CTE mismatch with respect to the rings affects preload change over temperature at least as much as sleeve material choice.
- Sleeve fit dominates preload variation compared to housing fit within the temperature range.
- Ball CTE dominates preload change at the hot extreme as the sleeve and housing fits loosen and no longer radially squeeze the outer rings.
- Silicon nitride provides benefits such as increased lubricant life, lower weight, and higher stiffness with the detriment of a significantly different CTE and corresponding change of preload with temperature.
- 25 degree contact angle provides lower operating contact stress with minimal loss of launch load capability (compared to 15 degree contact angle).
- Parametric exploration of the design space allows a better understanding of the effects and significance of each parameter.
- For critical or ultra-precision applications, do not immediately assume that commercial off-the-shelf components are the ideal solution. Fully investigate the design space for available alternatives. While there may be more time and expense invested in the initial design activity, savings will be forthcoming once mechanism integration and test phases have begun.

Acknowledgements

The authors would like to thank the production, verification and quality team at Barden, especially Douglas Stange, for their dedication to producing world-class bearings for OCI and engineers at BEI Precision for their expertise at measuring and evaluating precision spindle assemblies. We also acknowledge the OCI team that supported the effort as we worked through the lessons learned, as described in this paper and others. We finally acknowledge Nick Kwiatkowski and Tom Huber for their outstanding efforts during assembly.

References

[1] NASA Goddard Space Flight Center (2017). PACE. Retrieved from https://pace.gsfc.nasa.gov/

[2] “Keeping the PACE”, *The Critical Path*, Volume 25, Number 3, NASA Goddard Space Flight Center. Retrieved from https://fpd.gsfc.nasa.gov/critical_path/critical_path_17winter.pdf

[3] Tang, C., et al, “A Study on the Effects of Ball Defects on the Fatigue Life in Hybrid Ball Bearings”, Proceedings from the 42nd Aerospace Mechanisms Symposium, May 2014, Baltimore, MD.

[4] Park, W., et al, “Rolling Contact Fatigue and Load Capacity Tests of M62 Bearing Steel”, Proceedings from the 32nd Aerospace Mechanisms Symposium, May 1998, Cocoa Beach, FL.

[5] Leveille, A. and Ward, P., “Wear Potential due to Low EHD Films during Elevated Temperatures”, Proceedings from the 42nd Aerospace Mechanisms Symposium, May 2014, Baltimore, MD.
[6] Smith, D., et al, “REX 20/Si3N4 Control Moment Gyroscope Bearing Development”, Proceedings from the 32nd Aerospace Mechanisms Symposium, May 1998, Cocoa Beach, FL.